

# Angle-resolved bremsstrahlung isochromat spectroscopy of Cu(100) and Cu(110)

W. Altmann, V. Dose, A. Goldmann,\* U. Kolac, and J. Rogozik

*Physikalisches Institut der Universität, Am Hubland, D-8700 Würzburg, Germany*

(Received 3 October 1983)

Angle-resolved isochromat spectra from Cu(100) and Cu(110) have been measured. The results in terms of energy versus momentum dispersions are discussed and compared to theoretical data. This includes predictions on the basis of a one-step theory and predictions within the bulk direct-transition model. The experimentally obtained  $E(\vec{k})$  points on the high-symmetry axes  $\Gamma-\Delta-X$  and  $\Gamma-K-X$  are also compared to results from angle-resolved photoemission spectroscopy. The present bremsstrahlung data fit in very well into the photoemission data. In particular, deviations from theory show the same sign and magnitude in both data sets. This encourages the conclusion that corrections to the one-electron energies in photoemission and bremsstrahlung spectroscopy on copper stay well below an upper limit of 0.3 eV.

## I. INTRODUCTION

Angle-resolved ultraviolet bremsstrahlung isochromat spectroscopy (ARUBIS) detects radiative transitions between initially empty electron energy bands.<sup>1-4</sup> If the primary electrons are prepared with well defined momentum, the transitions take place at well defined points in  $\vec{k}$  space and may therefore be used to map energy versus momentum dispersions of the bands involved in the radiative transition. The technique resembles closely angle-resolved ultraviolet photoemission spectroscopy (ARUPS). The difference between the two spectroscopies is that in ARUPS one of the bands involved is always occupied while in ARUBIS both are empty. The important application of ARUBIS is to those cases where one of the bands involved lies in the otherwise inaccessible region between the Fermi and the vacuum level. Considering the development of ARUPS during the past decade, we dare forecast quite a promising future for ARUBIS.

The feasibility of ARUBIS was demonstrated last year by several groups employing different experimental techniques.<sup>3-5</sup> First, ARUBIS results from Cu(100), the "classical testing material" in ARUPS, were collected and interpreted very recently.<sup>4</sup> Meanwhile, intensity calculations for this surface are also available<sup>6</sup> which are based on the well known one-step-model of ARUPS. It is the aim of the present paper to continue—on the basis of high-quality data—the discussion initiated in Refs. 4 and 6.

Information about empty bands situated energetically above the vacuum level is inherently also contained in ARUPS since the relevant transition connects occupied initial states  $|i\rangle$  with empty final states  $|f\rangle$  via the matrix element  $\langle f|\vec{A}\cdot\vec{p}|i\rangle$ , where  $\vec{A}$  is the vector potential of the incident light and  $\vec{p}$  the momentum operator. ARUBIS is described by the formally identical matrix element, but with  $|i\rangle, |f\rangle$  now representing singly occupied initial and empty final states, respectively, and  $\vec{A}$  being the vector potential of the emitted radiation. It is therefore quite evident that conservation laws for energy and momentum and polarization selection rules for ARUPS apply as well to ARUBIS.

An important difference between the two spectroscopies arises if one considers corrections to the one-electron energies. Angle-resolved photoemission removes one electron from the system. Screening of the hole created by conduction electrons leads in principle to a relaxation shift of the undistorted ground-state energies. There is a long but so far unsettled debate in the literature about the possible size of this effect.<sup>7</sup> ARUBIS, on the other hand, adds an electron to the system and is therefore expected to create a relaxation shift of different magnitude and opposite sign. In an oversimplified atomic picture, the respective energetic deviations from the ground-state energy are those of a positive (ARUPS) and negative (ARUBIS) ion.

A comparison of empty band energies as determined from ARUPS and from ARUBIS, respectively, offers a very promising approach to the relaxation problem. In this work, for Cu(100) along  $\Gamma-\Delta-X$  we find excellent agreement between our bremsstrahlung and available ARUPS data.<sup>8</sup> Relaxation effects stay therefore below the limits dictated by the available experimental resolution. This is consistent with a very recent study of high-resolution ARUPS of Cu. The experimental results in that work<sup>9</sup> could be quite well described by band energies from Burdick's<sup>10</sup> ground-state calculation.

## II. EXPERIMENTAL

The isochromat spectrometer employed in this work has been described in detail elsewhere.<sup>11</sup> It is based on an energy-selective ultraviolet Geiger Müller counter<sup>12</sup> with pass energy of 9.7 eV. The electron angle of incidence with respect to the sample normal can be varied between  $\pm 45^\circ$ .

Light emitted by the sample is detected within an average collection angle of  $\bar{\alpha}=46^\circ$ . For normal electron incidence, an alternative geometry is available with reduced light collection angle  $\bar{\alpha}=22^\circ$ . Differences in the two types of normal-incidence spectra can thus be attributed to polarization of the emitted radiation.

The spectrometer is mounted in a standard ultrahigh vacuum system offering the usual facilities for sample preparation and characterization. The copper single-crystal samples were cleaned *in situ* by the usual argon ion

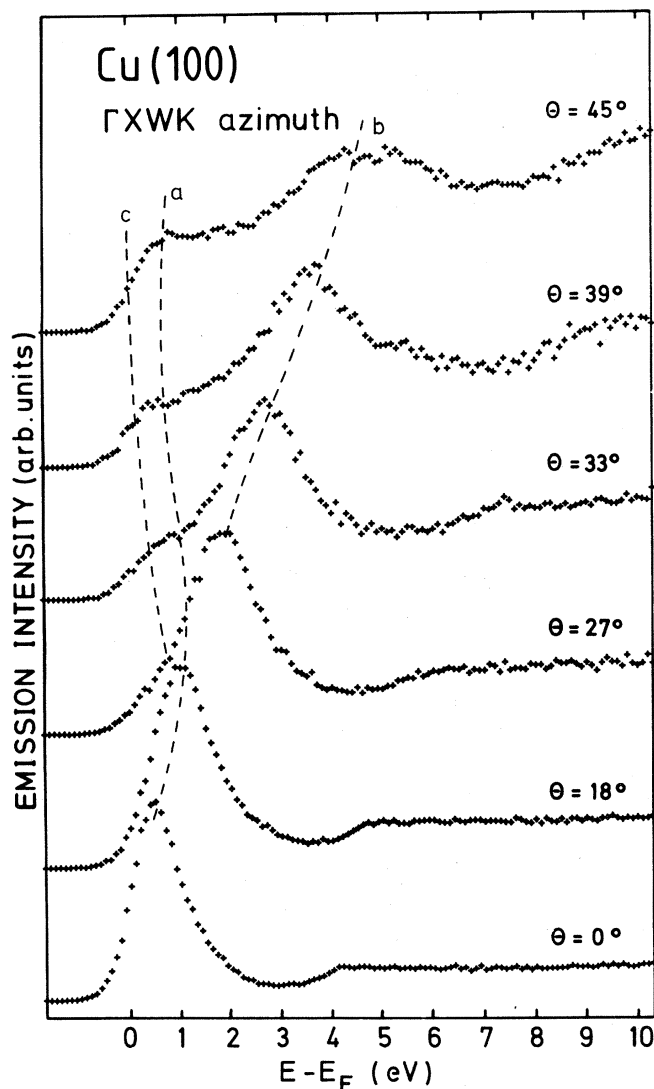


FIG. 1. Isochromat spectra for electrons incident at different polar angles  $\theta$  in the  $\Gamma XWK$  azimuth. Dashed lines indicate peak positions for bulk direct transitions predicted from Burdick's band structure.

etching and annealing until a very sharp low-energy electron diffraction (LEED) pattern with low background intensity was obtained. No contaminants could be detected within the limits of sensitivity of retarding field Auger analysis employing a glancing-incidence electron gun.

### III. RESULTS AND DISCUSSION

Typical isochromat spectra for electrons incident at different polar angles  $\theta$  in the  $\Gamma XWK$  azimuth are displayed in Fig. 1. When comparing our results to the corresponding data displayed in Fig. 6 of Ref. 4, several differences show up. First, at  $\theta=0^\circ$ , the peak ( $E=0.5$  eV) to valley ( $E=2.8$  eV) ratio is increased from about 2.3 in Ref. 4 to about 13 in the present work. Secondly, the prominent peak labeled *b* in Fig. 1 is observed up to  $\theta=45^\circ$ , while it disappears almost completely in Ref. 4 at  $\theta=29^\circ$ . Moreover, the peak *a* positions at  $\theta=0^\circ$  agree within 0.15 eV in both studies, but peak *b* shows different dispersion with  $\theta$ .

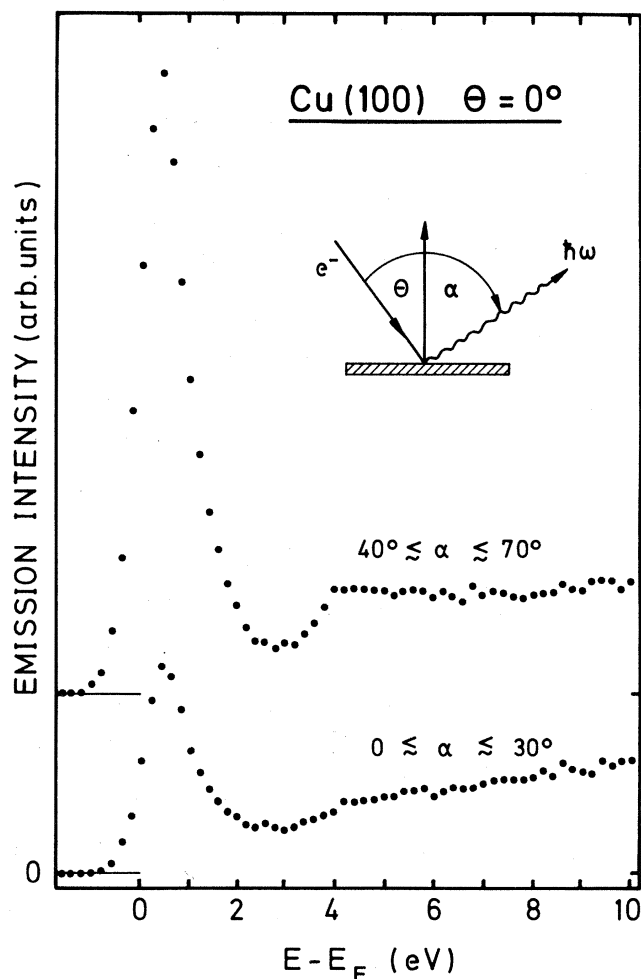


FIG. 2. Normal-incidence spectra from Cu(100) obtained with two different photon collection geometries. The intensity variations of the direct transition peak demonstrates the polarization of the emitted radiation.

For example, at  $\theta=29^\circ$ , the peak *b* energies differ by 0.8 eV. At present, we cannot offer explanations for these discrepancies. The rather good agreement in energy position at  $\theta=0^\circ$  rules out a very different calibration of  $E_F$ . Further, since the same radiation-detection principle is used in both experiments, the overall energy resolution is also comparable in both studies. Indeed, the half width at half maximum of the low-energy side of peak *a* at  $\theta=0^\circ$  is read from Fig. 6 of Ref. 4 to be 0.65 eV, and 0.52 eV from Fig. 1 of our work. This small apparent difference in resolution cannot explain the differences observed in the two sets of spectra. We can also rule out photon polarization effects due to different photon-collection geometries. This is demonstrated by Fig. 2 where we have collected isochromat spectra at normal incidence ( $\theta=0^\circ$ ) but at different average photon-emission angles  $\bar{\alpha}$ . Normal electron incidence locates the momentum of the bands involved on the  $\Gamma-\Delta-X$  high-symmetry axis in  $\vec{k}$  space. Symmetry requires<sup>13</sup> the initial state to be of symmetry  $\Delta_1$ . An inspection of the band structure<sup>10</sup> (see also Fig. 3) shows that there is only one  $\Delta_1$ -like final state available. Therefore, the  $\vec{A} \cdot \vec{p}$  operator in the matrix element must also

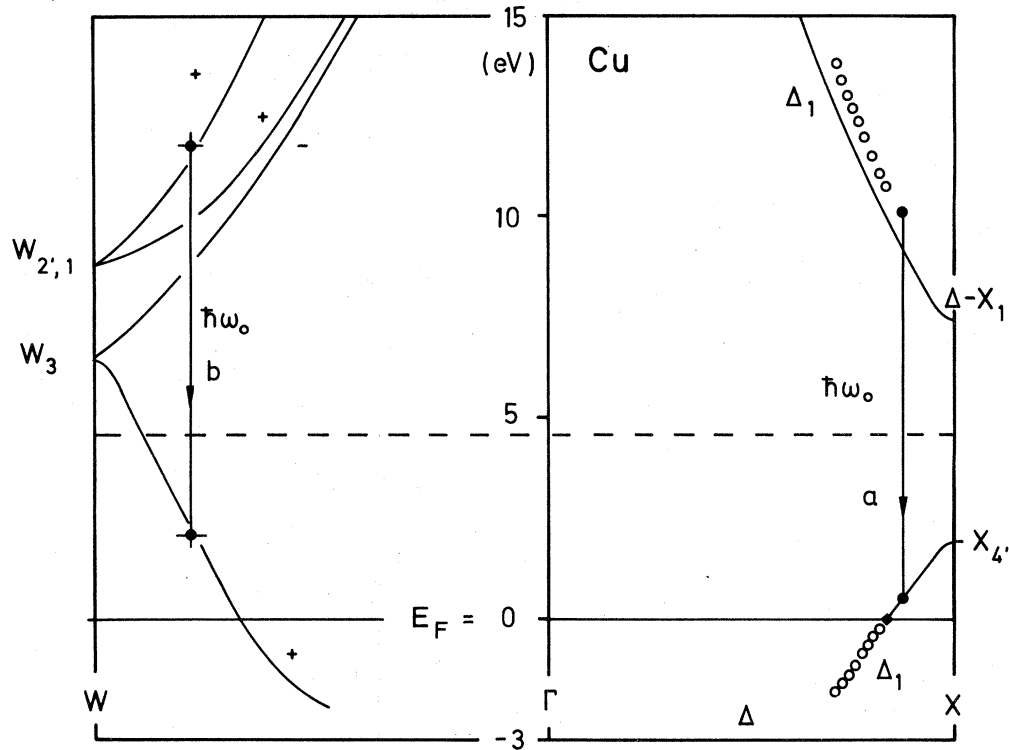


FIG. 3. Comparison of experimentally determined band energies to theoretical data from Burdick's band-structure calculation. Open circles indicate photoemission data.

possess  $\Delta_1$  symmetry.<sup>13</sup> The emitted photon must therefore be, in the limit of vanishing spin-orbit coupling, linearly polarized along the surface normal. Consequently, emission from the transition at  $\theta=0^\circ$  is strongly suppressed at small collection angles  $\alpha$ . This polarization effect is clearly brought out in Fig. 2. The normal-incidence data in Ref. 4 were obtained at an average collection angle of  $\bar{\alpha}=45^\circ$  and should therefore be quite similar to the upper spectrum in Fig. 2. We conclude that polarization effects cannot account for the observed intensity difference at  $\theta=0^\circ$ .

The result of Fig. 2 is interpreted in the right half of Fig. 3 where the solid circles locate the observed bremsstrahlung transition along  $\Gamma-\Delta-X$ . The open circles reproduce normal emission ARUPS results<sup>8</sup> for Cu(100). These have been located<sup>8</sup> along the  $\Delta(k_\perp)$  line using two rather reliable assumptions:

(i) The lower  $\Delta_1$  band crosses  $E_F$  at  $k_\perp=1.44 \text{ \AA}^{-1}$  as known from de Haas-van Alphen measurements.<sup>14</sup>

(ii) The slope of the lower band near  $E_F$  is known from ground-state band calculations. This is well justified since different available calculational procedures<sup>10,14,15</sup> yield the same slope within the required precision.

In order to make a self-consistent comparison of our result to the ARUPS data, the two assumptions listed above were used. The ARUPS data were extrapolated linearly through the de Haas-van Alphen data point shown as the filled diamond in Fig. 3. This extrapolation turned out to coincide with available theoretical band-structure calculations near the Fermi level. The intersection of the extrapolation straight line with the energy of the ARUBIS is

then automatically fixed in the upper  $\Delta_1$  band of Fig. 3. Figure 3 indicates a remarkable agreement of our result along  $\Delta$  with the experimental  $\Delta_1$  band as determined by ARUPS. We conclude that relaxation effects if present should be no larger than 0.2–0.3 eV. Also plotted in Fig. 3 are results of Burdick's<sup>10</sup> calculation which runs slightly below the experimental points in the upper  $\Delta_1$  band and shows excellent agreement for the lower  $\Delta_1$  band. A more recent calculation<sup>16</sup> which takes relativistic effects into account places the upper  $\Delta_1$  band intermediate between Burdick's result and the experimental points. The important point we want to emphasize here is that ARUPS and ARUBIS data, evaluated according to the same recipe, show excellent agreement. This data treatment, however, does not allow a decision as to which calculated band structure is "the best." Also shown in Fig. 3 is an experimental result (open triangle) for the energy of the  $X_1$  critical point at 8.0 eV. The latter value was chosen to be the average of results from ARUPS ( $7.9 \pm 0.1$  eV) (Ref. 8) and from angle-resolved secondary electron emission spectroscopy ( $8.1 \pm 0.1$  eV).<sup>17</sup> The energetic position of  $X_1$  fits in nicely with other experimental observations. Since secondary electron spectroscopy probes just the same singly occupied states as ARUBIS, the agreement of the  $X_1$  energy with the ARUPS result again indicates relaxation shifts definitely smaller than 0.2–0.3 eV.

The energetic position of the most prominent peak in all our results is plotted in Fig. 4 versus  $k_\parallel$ . The simplest description of these data is in terms of radiative transitions between plane-wave states interacting by only one pseudopotential coefficient. This "two-band-model" has

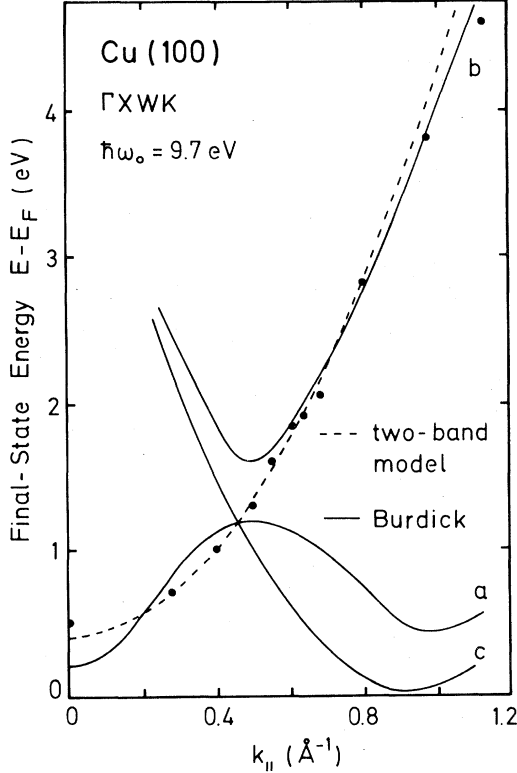


FIG. 4. Solid dots are the experimentally obtained dispersion of the prominent peak in Fig. 1. The dashed line shows the prediction of a two-band approximation. Solid lines indicate possible final-state energies derived from a full band-structure calculation.

been described in Ref. 4. It predicts an energy dispersion of  $E = (\hbar^2/2m)k_{\parallel}^2 + c$ , where  $E$  is the final-state energy,  $m$  the free-electron rest mass, and  $c$  is a constant. If we chose  $c = 0.4$  eV, the agreement with our data is remarkably good for this simple model. We also calculated the final-state energy  $E$  predicted by Burdick's band structure.<sup>10</sup> The result (which essentially agrees with Ref. 4) is given by the solid lines labeled *a*, *b*, and *c* in Fig. 4. These curves take into account all points in the  $\Gamma XWK$  plane where two energy bands 9.7 eV apart exist, irrespective of the matching conditions to the incident electron and the magnitude of the optical-transition matrix element. As seen from Fig. 4, only branch *a* contributes appreciably below  $k_{\parallel} = 0.5 \text{ \AA}^{-1}$ , while above  $k_{\parallel} = 0.5 \text{ \AA}^{-1}$  the prominent intensity is transferred to branch *b*. The intense peaks in Fig. 1 have been labeled accordingly. The results of Fig. 4 clearly indicate that the incoming electrons couple preferentially to those bulk initial states which are free-electronlike in agreement with conclusions of Ref. 4. In other words, the results are governed by "primary cone incidence" in analogy to "primary cone emission" in ARUPS in Mahan's sense,<sup>18</sup> and bulk umklapp processes do not play an important role here. The data points in Fig. 4 show a slight deviation from curve *a* for small  $k_{\parallel}$  values, fully consistent with the observed deviation within the upper  $\Delta_1$  band at  $k_{\parallel} = 0$  in Fig. 3. Above  $k_{\parallel} = 0.5 \text{ \AA}^{-1}$ , the agreement of the experimental points in Fig. 4 with branch *b* is much better than below: this reflects the

fact that the ARUBIS initial state becomes more free-electronlike with increasing energy.

We may therefore also resort to the common practice in ultraviolet photoelectron spectroscopy (UPS) and describe the bulk initial state  $|i\rangle$  of branch *b* by a free-electronlike band

$$E_i = (\hbar^2/2m)(\vec{k}_{\parallel}^2 + \vec{k}_{\perp}^2) + E_0.$$

Since  $\vec{k}_{\parallel}$  is fixed by the experimental parameters, this approach allows a unique  $\vec{k}$  space location of an observed transition by  $\vec{k}_{\parallel}$  and  $\vec{k}_{\perp}$  (as defined in the extended-zone scheme). As parameters of the model we use a free-electron rest mass  $m$  and  $E_0 = -7.5 \pm 0.5$  eV (with respect to  $E_F$ ) for the inner potential. This choice of  $m$  and  $E_0$  allows an excellent description of off-normal ARUPS data<sup>19,20</sup> taken in the  $\Gamma XWK$  mirror plane of Cu(100), if Burdick's<sup>10</sup> calculated initial bands are used in combination with free-electron-like final states. One of our experimental results is shown in the left part of Fig. 3 where we plotted a transition located just on the  $\Gamma-W$   $\vec{k}$ -space axis. For the same direction, we also plot the energy bands as obtained by an interpolation of Burdick's eigenvalues.<sup>21</sup> The good agreement observed supports our earlier conjecture that ARUPS and ARUBIS may be described within the present error bars by just the same upper energy band. However, in both results, plotted in Fig. 3, model assumptions enter the  $\vec{k}$ -space localization of our data, and this is of course unsatisfactory. Clearly, an "absolute" determination of  $k_{\perp}$ , e.g., by a triangulation method<sup>22,23</sup> is highly demanded. Such work is now in progress in Würzburg.

Our experimental results do not reveal the gap predicted in Fig. 4 between branches *a* and *b*. When this gap is crossed at  $\theta = 23^\circ$ , no change in intensity is observable. The latter fact is seen more clearly in Fig. 5(a), where we have plotted spectra at finer angular increments than in Fig. 1. The closing of the gap is essentially an effect of intrinsic resolution  $\Gamma$ . In our particular case, the observed peak width, although difficult to define precisely in the spectra, is  $\Gamma_{\text{obs}} \approx 1.3$  eV. The overall resolution of the experiment, determined essentially by electron gun and photon counter, amount to  $\Gamma_{\text{exp}} = 0.82$  eV.<sup>1</sup> The resulting limits for  $\Gamma$  obtained from  $\Gamma^2 + \Gamma_{\text{exp}}^2 \leq \Gamma_{\text{obs}}^2 \leq (\Gamma + \Gamma_{\text{exp}})^2$  are  $0.5 \leq \Gamma/\text{eV} \leq 0.9$ . The actual intrinsic width is therefore safely larger than the predicted gap of 0.45 eV. From these results, we conclude that larger gaps should be readily observable by ARUBIS in that range of initial-state energies.

We mention in this context that gaps of widths 2–5 eV are also clearly identified in angle-resolved secondary electron emission from different  $W$  faces.<sup>24</sup> In the latter technique, the electron coupling through the surface is exactly the inverse of the corresponding step in ARUBIS.

In Fig. 5(b), we have reproduced the results of a recent one-step-model calculation<sup>25</sup> for ARUBIS from Cu(100) with kinematical parameters comparable to our data in Fig. 5(a). Some interesting conclusions may be drawn from a comparison between both sets of data:

(a) The calculated energy positions are in excellent agreement ( $\pm 0.1$  eV) with our data. This is as expected

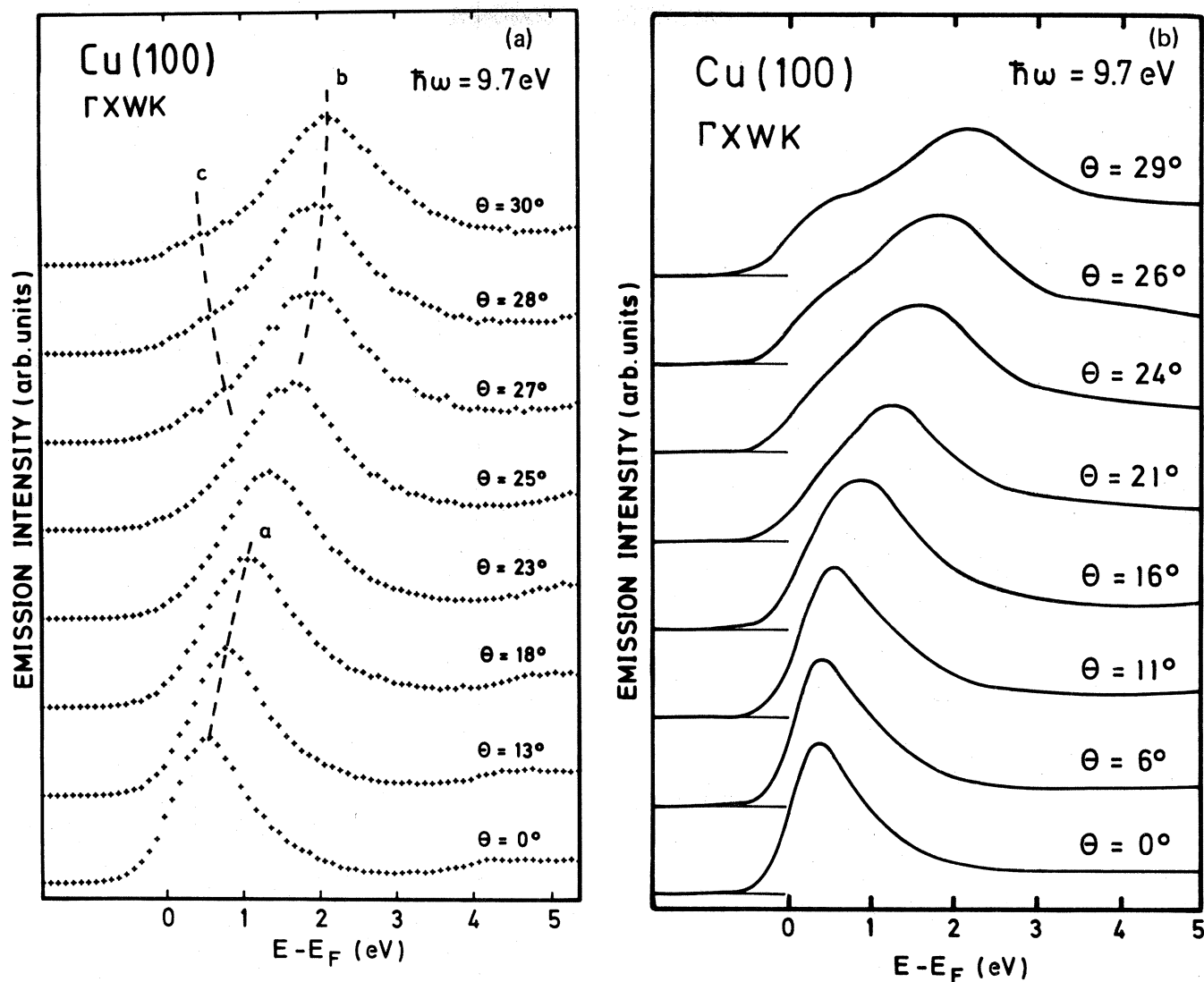


FIG. 5. The left panel shows experimentally obtained isochromats as in Fig. 1 but at finer angular increments. The right-hand panel shows theoretical spectra calculated on the basis of a one-step theory.

since the results of Fig. 5(b) (Ref. 6) are essentially based also on Burdick's potential.<sup>10</sup> Thus, the slight disagreement of the calculated energy positions (up to 0.5 eV) with respect to the experimental data presented in Ref. 4 is removed.

(b) At normal electron incidence, the peak [at 0.5 eV in Fig. 5(a)] to valley (at 2.8 eV) ratio is about 13 in the experimental data, in reasonable agreement with the calculated ratio of about 8.

Let us now focus on the structures observed in Figs. 1 and 5(a) at final-state energies below 1 eV. We tentatively explain them by transitions from branches labeled *a* and *c* in Fig. 4 in the range of  $k_{||} > 0.5 \text{ \AA}^{-1}$ . It is evidently difficult to extract experimental peak positions. We have instead calculated from Fig. 4 the peak positions to be expected for the experimental incidence angles, and indicated them in Figs. 1 and 5(a) by the dashed lines labeled *a* and *c*. It is obvious that the experimental results are consistent with our assignment.

The foregoing interpretation is also consistent with oth-

er information. Calculated momentum matrix elements for bulk transitions<sup>4</sup> indicate the intensity of feature *a* should decrease rapidly to zero for  $k_{||} \rightarrow 0.7 \text{ \AA}^{-1}$ . However, simultaneously the intensity of *c* increases monotonically, starting from zero at  $k_{||} \approx 0.4 \text{ \AA}^{-1}$ , until at  $k_{||} = 0.87 \text{ \AA}^{-1}$  transitions *b* and *c* are expected to be of comparable strength. The intensity and energy position of *c* in Fig. 5(a) are reasonably explained. However, the spectrum obtained at  $\theta = 45^\circ$  shown in Fig. 1 suggests an interpretation of the prominent step around 0.8 eV by transition *a* which has no transition strength according to the bulk matrix element.<sup>4</sup> Therefore we prefer an interpretation which assumes strong intensity contributions to the structures under consideration in terms of density-of-states (DOS) transitions, reflecting the one-dimensional DOS along the line  $\vec{k}_{||} = \text{const}$  as defined by the experimental choice of  $\theta$  and  $E$ . Such DOS transitions can occur only in the surface region, where relaxation of the selection rule takes place. The surface, however, is not taken properly into account in the bulk momentum matrix

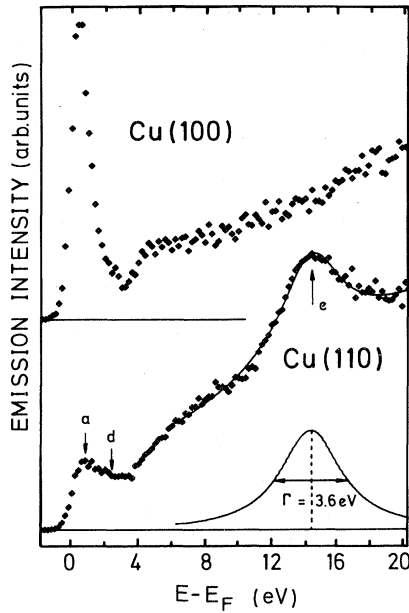


FIG. 6. Normal-incidence spectra from Cu(100) and Cu(110).

element.<sup>4</sup> In principle, DOS transitions are automatically included in one-step-model calculations. But obviously they are not resolved in Ref. 6.

Let us now turn our attention to the normal-incidence spectrum obtained from Cu(110) which is displayed in Fig. 6. As compared to the normal-incidence spectrum from Cu(100), which is also shown for comparison, there is no strong emission peak in the low-energy region. We only observe a weak structure positioned at 0.7 eV (labeled *a*) and, near the detection limits, a shoulder *d* at about 2.5 eV. At  $(14.3 \pm 0.3)$  eV a rather prominent peak *e* is resolved. After a linear-background subtraction, a Lorentzian fit to this structure yields a width of  $\Gamma \approx 3.6$  eV. This width is of the order of magnitude expected<sup>8</sup> for the lifetime broadening of excited energy bands in the range 20–30 eV above  $E_F$ . Thus, peak *e* is a candidate for a direct transition.

Normal incidence on Cu(110) localizes the observed transitions on the  $\Gamma$ - $K$ - $X$  direction in  $k$  space if we assume that primary cone incidence is dominant also for the (110) face of Cu. Unfortunately, Burdick's band-structure calculation does not extend to sufficiently high initial-state energies. We use instead the recent relativistic calculation of Eckhardt *et al.*<sup>16</sup> which is reproduced along the  $\Gamma$ - $K$ - $X$  direction in Fig. 7. We mention here that the overall agreement of this calculation with Burdick's results is remarkably good above  $E_F$ .

Inspection of Fig. 7 shows that the observed three peaks can unambiguously be correlated with transitions between specific energy bands, except of course for the indeterminacy of  $k_{\perp}$ . In the following discussion, we number the bands according to increasing energy at  $X$ . If we assume that transition *a* ends at 0.8 eV on the calculated band 1 (solid circle), the corresponding initial state is placed on band 3, and the final state is located at  $1.38 \text{ \AA}^{-1}$  away from  $\Gamma$ . The length of the  $\Gamma$ - $K$ - $X$  axis is  $2.46 \text{ \AA}^{-1}$ . The same procedure locates transition *d* also on

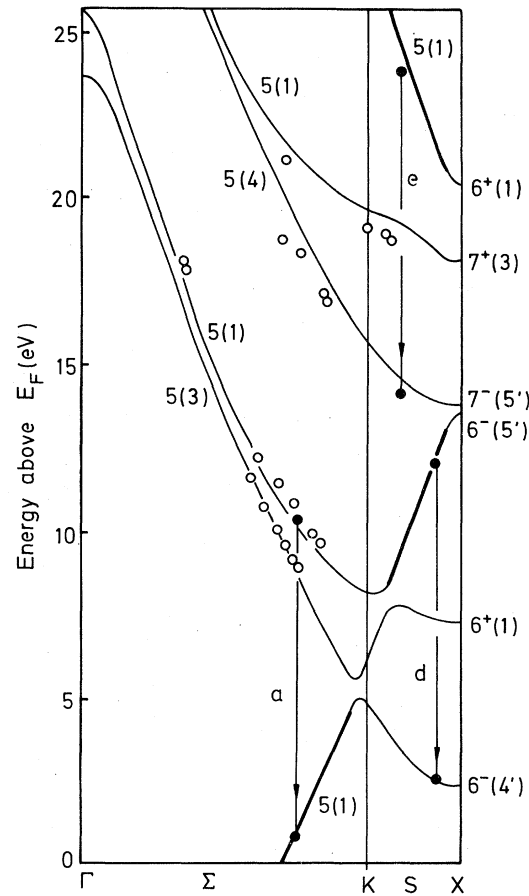


FIG. 7. Comparison of experimentally determined band energies to the copper band structure along  $\Gamma$ - $K$ - $X$ . Open circles are photoemission data, full dots are the results of this work.

bands 1 and 3, but at a different  $k_{\perp} = 2.30 \text{ \AA}^{-1}$ . Similarly, transition *e* connects bands 6 and 4.

To explain the different intensities, we refer to the discussion of the Cu(100) results: Good  $k_{\perp}$  matching to the incoming beam requires the bulk initial state to possess predominant free-electron-like character. In Fig. 7 we have characterized the corresponding primary cone bands by heavy lines. Clearly, transition *a* does not satisfy the matching condition. It probably contributes only via DOS contributions. However, the matching condition is clearly satisfied for transition *d*. The band structure determines, in connection with the experimentally observed energy, the value of  $k_{\perp} = 2.30 \pm 0.15 \text{ \AA}^{-1}$ , and a free-electron-like final band with the parameters chosen as above would require  $k_{\perp} = 2.26 \text{ \AA}^{-1}$ . Therefore the strong suppression of transition *d* must have its reason in a very small matrix element. This is not unreasonable, since that transition occurs very near to the  $X$  point. Exactly at  $X$ , transitions between bands 3 and 1 are forbidden by symmetry, since both critical points have identical parity assignment, while the electric dipole transition requires a parity change. From the experimental results, we may therefore conclude that near  $X$  no appreciable components of different parity are admixed to the wave functions in bands 3 and 1. To localize transition *e* in  $\vec{k}$  space, we have used again the free-electron-like initial state. This model yields

$k_{\perp} = (2.86 \pm 0.02) \text{ \AA}^{-1}$  in the extended zone, and the data points (solid circles) are correspondingly arranged in Fig. 7 (reduced zone).

Also plotted in that figure are several results obtained from ARUPS by different authors<sup>9</sup>. Again we observe an excellent agreement between the ARUBIS and ARUPS information. For example, within band 3, the ARUPS data are positioned slightly above the calculated band, and the same is true for the isochromat initial state. Also, in band 4, where the ARUPS data now appear somewhat below the theoretical position, the same behavior is found with

the present result. We thus conclude that also for Cu(110) there is strong evidence that excited-state relaxation effects in ARUPS are much smaller than the resolution obtained in the present work.

#### ACKNOWLEDGMENTS

This research has been financially supported by the Deutsche Forschungsgemeinschaft and a special University grant provided by R. Günther. We have benefited from numerous discussions with Dr. H. Scheidt.

---

\*Permanent address: Laboratorium für Festkörperphysik der Universität, D-4100 Duisburg, Germany.

<sup>1</sup>V. Dose, *Prog. Surf. Sci.* **13**, 225 (1983).

<sup>2</sup>J. B. Pendry, *J. Phys. C* **14**, 1381 (1981).

<sup>3</sup>G. Denninger, V. Dose, and H. P. Bonzel, *Phys. Rev. Lett.* **48**, 279 (1982).

<sup>4</sup>D. P. Woodruff, N. V. Smith, P. D. Johnson, and W. A. Royer, *Phys. Rev. B* **26**, 2943 (1982), and references therein.

<sup>5</sup>F. J. Himpsel and Th. Fauster, *Phys. Rev. Lett.* **49**, 1583 (1982).

<sup>6</sup>G. Thörner and G. Borstel, *Solid State Commun.* **47**, 329 (1983).

<sup>7</sup>Critical point energies from various band-structure calculations differ by up to 0.8 eV from experimental photoemission results. Whether such discrepancies signal relaxation effects or result from shortcomings of the one-electron model remains open to discussion, see R. Courths, V. Bachelier, B. Cord, and S. Hüfner, *Solid State Commun.* **40**, 1059 (1981).

<sup>8</sup>D. E. Eastman, J. A. Knapp, and F. J. Himpsel, *Phys. Rev. Lett.* **41**, 825 (1978).

<sup>9</sup>R. Courths, B. Cord, H. Wern, and S. Hüfner, *Phys. Scr.* **T4**, 144 (1983).

<sup>10</sup>G. A. Burdick, *Phys. Rev.* **129**, 138 (1963).

<sup>11</sup>V. Dose, M. Glöbl, and H. Scheidt (unpublished).

<sup>12</sup>G. Denninger, V. Dose, and H. Scheidt, *Appl. Phys.* **18**, 375 (1979).

<sup>13</sup>J. Hermanson, *Solid State Commun.* **22**, 9 (1979).

<sup>14</sup>J. F. Janak, A. R. Williams, and V. L. Moruzzi, *Phys. Rev. B* **11**, 1522 (1975).

<sup>15</sup>N. V. Smith and L. F. Mattheis, *Phys. Rev. B* **9**, 1341 (1974).

<sup>16</sup>H. Eckhardt, L. Fritsche, and J. Noffke, (unpublished).

<sup>17</sup>K. K. Kleinherbers and A. Goldmann (unpublished).

<sup>18</sup>G. D. Mahan, *Phys. Rev. B* **2**, 4334 (1970).

<sup>19</sup>R. Courths, V. Bachelier, B. Cord, and S. Hüfner, *Solid State Commun.* **40**, 1059 (1981).

<sup>20</sup>D. Westphal and A. Goldmann, *Surf. Sci.* **131**, 92 (1983); **131**, 113 (1983), and references therein.

<sup>21</sup>Data taken from E. Dietz, dissertation, University of Frankfurt, Frankfurt am Main, 1976 (unpublished), and private communication.

<sup>22</sup>E. O. Kane, *Phys. Rev. Lett.* **12**, 97 (1964).

<sup>23</sup>P. Heimann, H. Miosga, and H. Neddermeyer, *Solid State Commun.* **29**, 463 (1979).

<sup>24</sup>R. F. Willis, *Phys. Rev. Lett.* **34**, 670 (1975).

<sup>25</sup>The data of Ref. 6 have been truncated at  $E_F$ . The resulting step has been smeared with our apparatus function.